

Effects of Pauli paramagnetism on superconducting vortex phase diagram in strong fields

Hiroto Adachi and Ryusuke Ikeda

Department of Physics, Kyoto University, Kyoto 606-8502, Japan

(dated: January 9, 2022)

The Ginzburg-Landau (GL) functional and the resultant phase diagram in strong fields where the Pauli paramagnetic depairing is not negligible are examined in details by assuming the weak coupling BCS model with a $d_{x^2-y^2}$ -like pairing. In contrast to previous works on the same subject for spin-singlet pairings in which the orbital depairing effect was not treated consistently with the paramagnetic depairing, the temperature at which the mean field (MF) transition at H_{c2} changes into a discontinuous one lies much above another temperature at which the $H_{c2}(T)$ and a second order transition curve $H_{FFLO}(T)$ between an FFLO-like and the ordinary vortex solids branch, and $H_{FFLO}(T)$ decreases upon cooling. Based on these MF results, details of a real phase diagram near $H_{c2}(T)$ -line are examined in terms of Monte Carlo simulation, and it is found that the MF discontinuous transition is changed due to the fluctuation into a crossover which is nearly discontinuous in systems with weak enough fluctuation. These results induced by the paramagnetic depairing are consistent both with recent observations of the MF discontinuous behavior and $H_{FFLO}(T)$ in the heavy fermion superconductor CeCoIn₅ with weak fluctuation and with their absence in organic materials with strong fluctuation.

INTRODUCTION

Traditionally, effects of Pauli paramagnetism on superconductors with a spin-singlet Cooper-pairing have been discussed by simply focusing on two energy scales [1, 2]; the superconducting (SC) condensation energy and the Zeeman energy preventing the singlet pairing. This is a reasonable explanation on the first order transition (FOT) in an exceptional case with no orbital depairing creating field-induced vortices, i.e., a thin-film superconductor in parallel fields [3]. Further, there is also a possibility of a structural transition within the Meissner phase into the so-called FFLO state [4, 5] with a periodic modulation, induced by the spin depairing, of the SC order parameter. However, the orbital depairing effects, i.e., the vortices are inevitably present in most of cases of a type II superconductor under a strong field, including a layered material under a field parallel to the superconducting layers [7]. Hence, we encounter quite a different issue from that in the works [1, 2, 4, 5, 6], that is, effects of the paramagnetic depairing on the vortex state which has no Meissner response. Clearly, treating in this case the orbital depairing as a perturbation for the case with no orbital depairing is not valid.

At present, it is well understood [8, 9] that, in lower fields where the paramagnetic depairing is negligible, the H - T phase diagram for the vortex states is drastically changed by including the superconducting fluctuation neglected in the mean field (MF) approximation. A typical one among such drastic fluctuation effects is the fact that the second order MF transition at H_{c2} is not realized as a consequence of the fluctuation and gives way to a weak first order transition lying below H_{c2} between the vortex solid and the vortex liquid region which needs not be distinguished from the normal state. At least theoretically,

it is important [10] to extend this issue to the strong field region in which the spin depairing is not negligible and the MF transition at H_{c2} may be discontinuous.

Through previous MF works on the vortex states of Pauli-limited superconductors [11, 12, 13], however, one notices that even the H - T phase diagram in the MF approximation is an unsettled issue. For instance, a FOT induced by the spin depairing was expected through a calculation in dirty limit [13], to the best of our knowledge, contrary to the experimental facts. Further, even in the clean limit, there are no consensus on the MF phase diagram. In strong fields of our interest, any Meissner phase (i.e., any phase occurring with no orbital depairing) is not possible, and we expect just some vortex solids, such as the ordinary solid consisting of straight vortex lines and an FFLO-like solid state with a periodic modulation along the applied field, as SC ground states in the pure limit with no defects leading to a vortex-pinning. Let us call a transition curve between the above-mentioned two solid states as $H_{FFLO}(T)$. In ref.[11], the transition at H_{FFLO} was argued to be of first order with no detailed calculation, while it was obtained as a second order one in ref.[12] where the orbital depairing represented by the gauge-invariant gradient is treated perturbatively. Further, the temperature T at which the MF transition at H_{c2} changes into a discontinuous one was concluded there [12] to lie much below another temperature T_{FFLO} at which $H_{FFLO}(T)$ and $H_{c2}(T)$ branch. In addition, $H_{FFLO}(T)$ -line is often suggested to be insensitive to T . We note that all of conflicting results raised above were obtained in the same model, i.e., the simplest weak-coupling BCS model.

In the present paper, we first reexamine the MF calculations in the weak-coupling BCS model primarily in the region where the SC order parameter is described with in

the lowest Landau level (LLL) and show, by treating the two depairing effects on the same footing, that most of the previous MF results mentioned above are changed. Our analysis is essentially different from that in ref.[12] in that the gauge-invariant gradient is fully incorporated. Except in the case with a continuously large Maki parameter, this treatment is needed particularly in the high H and low T region where the paramagnetic depairing plays significant roles, although, instead, multiple numerical integrals have to be performed to accomplish such a full treatment. Further, bearing a comparison with data in real systems in mind, a weak impurity scattering should be incorporated because the $H_{FFLO}(T)$ line which may appear in high H and low T is easily suppressed by the impurity strength. Consequently, the MF phase diagram is determined by a competition among the two depairing effects and the impurity strength. We find that, in quasi-two-dimensional superconductors under magnetic fields perpendicular to the SC layers, the temperature T always lies above other two characteristic temperatures T_{FFLO} and T_{next} below which the vortex solid will be described by the next lowest Landau level (LL). This result will be compared with the high field phase diagram of the heavy fermion superconductor CeCoIn₅ reported very recently [14], and they are found to be consistent with each other.

Next, we also explain here results of our Monte Carlo simulations on a GL model justified at the microscopic level performed by focusing on the high fields in which a FOT at H_{c2} (MF-FOT) must occur in the MF approximation completely neglecting the fluctuation. As explained elsewhere [10], the strong MF-FOT induced by the spin depairing is expected theoretically to never occur in real systems with fluctuation. Otherwise, the high field portion of the H-T phase diagram would not become compatible with its low field portion because the absence of the second order MF transition at H_{c2} in lower fields is already well-established. The only transition in the case with no pinning disorder should be the melting transition of a vortex solid. In the present case with a MF-FOT, however, the GL model needs to have nonlinear terms other than the quartic term, and this fact makes an analytic study more involved. For this reason, we have chosen to perform Monte Carlo simulations to examine the true phase diagram. Our results are consistent with the theoretical prediction and reveal that the above-mentioned MF-FOT at H_{c2} is changed into a crossover from a normal state into a vortex liquid region broadening with increasing fluctuation. Together with the impurity-induced disappearance of the MF-FOT, this fluctuation-induced broadening of the sharp behavior reflecting the MF-FOT explains why the nearly discontinuous behavior at H_{c2} has not been observed so far in, except the recent observations in CeCoIn₅ [14, 15, 16, 17, 18], most of bulk type II superconductors with a spin-singlet pairing. On the other hand, we find

that, in spite of the absence of the genuine FOT at H_{c2} , a hysteresis may appear near H_{c2} in numerical simulations for cases with weaker fluctuation as a result of an incomplete relaxation at finite time scales in numerical simulations. To clarify this argument, the corresponding results for a one-dimensional GL model in zero field, which has no superconducting transition, will be presented. In specific heat measurements on CeCoIn₅ [14], a small hysteresis accompanying the FOT-like behavior at H_{c2} begins to appear upon cooling at some low temperature in contrast to the resistivity data [18] at a lower temperature. Since there is no evidence that this onset of hysteresis is related to another phase transition and real specific heat measurements as well as numerical experiments are not necessarily performed at a true thermalequilibrium, the experimental hysteresis seen only in the specific heat data at low enough temperatures is consistent with our scenario based on the absence of a genuine FOT at H_{c2} .

This paper is organized as follows. In x2, we explain our microscopic derivation of the GL functional and discuss the disorder dependence of the resulting MF phase diagram. In x3, our simulation results are explained in details. In x4, the obtained result is compared with the observations in CeCoIn₅. We use the unit $\hbar = c = 1$ throughout the manuscript.

QUADRATIC TERM

Following Klemm et al.[19], we introduce a BCS Hamiltonian for a quasi-two dimensional (2D) superconductor under a nonzero magnetic field

$$H = H_0 + H_J - \frac{g}{2} \sum_{ij} \frac{d^2 q_p}{(2\pi)^2} B_j^y(q_p) B_j(q_p) \quad (1)$$

Here, g is the attractive interaction strength, $\psi_j(r_p) = (1/s) \sum_{p_p} a_j(p_p) e^{ip_p r_p}$ is the annihilation operator of a quasi-particle with spin s ($= +1$ or -1) at the in-plane position r_p on the j -th plane, and s and A is the interlayer spacing and the area of a layer, respectively. The pair-field operator is defined by $B_j(q_p) = \sum_{p_p} w_p a_j(p_p) a_j(p_p^+)$, where w_p is the orbital part of the pairing-function and, in the case of $d_{x^2-y^2}$ -pairing, is written as $\frac{p_x^2 - p_y^2}{2(p_x^2 + p_y^2)}$, where \hat{p} is the unit vector in the p_p direction, and p_p implies $p_p = q/2$. The first term H_0 in eq.(1) represents in-plane motions of quasi-particles,

$$H_0 = s \sum_{ij} \frac{d^2 r_p}{(2\pi)^2} \psi_j^y(r_p) \frac{(\nabla_{r_p}^2 + \frac{1}{2m})}{2m} \psi_j(r_p) + \sum_{ij} \psi_j^y(r_p) u_j(r_p) \frac{1}{I} \psi_j(r_p); \quad (2)$$

where $I = \phi_0 H$ is Zeeman energy, and m is the effective mass of a quasi-particle. The strength of the param-

agnetic depairing is measured by $H_{c2}^{\text{orb}}(0) = 2 T_{c0}$ corresponding to the Maki parameter except a numerical factor, where $H_{c2}^{\text{orb}}(T)$ is the MF transition curve in the case neglecting the paramagnetic depairing, and T_{c0} is the $H = 0$ transition temperature. The random potential $u_j(\mathbf{r}_?)$ obeys the following Gaussian ensemble: $\overline{u_j(\mathbf{r}_?)} = 0$, $\overline{u_j(\mathbf{r}_?)u_{j^0}(\mathbf{r}_?^0)} = (\mathbf{r}_? - \mathbf{r}_?^0)_{jj^0} = 2N(0)$, where $N(0)$ is a 2D density of state at the Fermi surface, and τ^{-1} the elastic scattering rate. The second term represents the inter-plane hopping,

$$H_J = \frac{J_S}{2} \sum_{\mathbf{r}_?} \sum_{\mathbf{r}_?'} \psi_{\mathbf{r}_?}^\dagger \psi_{\mathbf{r}_?'} + H.c. \quad (3)$$

where $H.c.$ denotes Hermitian conjugate. Since we are interested in a field region where electrons have a much larger cyclotron radius than the average distance between the quasiparticles, we use the familiar quasi-classical approximation for the single-particle propagator:

$$G_{\mathbf{r}}^H(\mathbf{r}; \mathbf{r}^0) = G_{\mathbf{r}}^{H=0}(\mathbf{r} - \mathbf{r}^0) e^{i\mathbf{p} \cdot \mathbf{r}} e^{i\mathbf{p} \cdot \mathbf{r}^0} \quad (4)$$

Here the Green's function in zero field, $G_{\mathbf{r}}^{H=0}(\mathbf{r})$, is given as the Fourier transform of the expression

$$G_{\mathbf{r}}(\mathbf{p}) = i^{\mathbf{p} \cdot \mathbf{r}} \left[\frac{1}{p_z} + J \cos(p_z s) \right] \quad (5)$$

where $\mathbf{p} = \mathbf{p} + s\mathbf{p}_z = (2\pi/\ell) \mathbf{p}$, and $s = \text{sgn}(\mathbf{p})$. Through the familiar Stratnovich-Hubbard procedure to introduce the pair-field, we can construct a GL functional. The quadratic term is given by

$$F_2 = \sum_{\mathbf{q}_z} \sum_{\mathbf{r}_?} \psi_{\mathbf{r}_?}^\dagger(\mathbf{q}_z) \frac{1}{\mathcal{V}} \hat{K}_2(\mathbf{q}_z) \psi_{\mathbf{r}_?}(\mathbf{q}_z); \quad (6)$$

where $\mathbf{r}_? = i\mathbf{r}_? + (2\pi/\ell)\mathbf{p}$, $\mathbf{p} = \mathbf{p} + s\mathbf{p}_z$ is the ux quantum, $\mathbf{p}_z = (sN_{\text{layer}})^{-1/2} \mathbf{p}_z$, $\psi_{\mathbf{r}_?}(\mathbf{q}_z) \sim e^{i\mathbf{q}_z \cdot \mathbf{r}_?}$ denotes the pair-field on the j -th SC plane, N_{layer} is the number of SC planes, and the operator \hat{K}_2 in the pure limit ($\ell \rightarrow \infty$) is simply given by

$$\hat{K}_2(\mathbf{q}_z) = 2N(0)T \sum_{\mathbf{p}} \hat{D}_d(2\mathbf{p});$$

$$\hat{D}_d(2\mathbf{p}) = \frac{1}{N(0)} \sum_{\mathbf{p}} \psi_{\mathbf{p}}^\dagger \psi_{\mathbf{p}} G_{\mathbf{p}}(\mathbf{p}) G_{\mathbf{p}}(\mathbf{p} + \mathbf{q}_z) \quad (7)$$

Here, the notation $\sum_{\mathbf{p}} = \sum_{\mathbf{p}} \frac{d^2 p_z}{(2\pi)^2} \frac{H}{2} \frac{d(p_z s)}{2}$ was used. In the impure case, there are also contributions from the impurity-ladder vertex corrections, and $\hat{D}_d(2\mathbf{p})$ should be replaced as follows:

$$\hat{D}_d(2\mathbf{p}) \rightarrow \hat{D}_d(2\mathbf{p} + 1) + \hat{E}_d(2\mathbf{p}) \frac{1}{\hat{D}_s(2\mathbf{p})} \hat{E}_d(2\mathbf{p}) \quad (8)$$

where $\mathbf{p} = (2\pi/\ell)\mathbf{p}$, and \hat{D}_s and \hat{E}_d are defined by replacing $\psi_{\mathbf{p}}^\dagger \psi_{\mathbf{p}}$ in eq.(7) into 1 and $w_{\mathbf{p}}$ respectively. In the dirty limit with $2T_{c0} \gg 1$, the impurity vertex correction expressed by \hat{D}_s in the second term becomes important, although the superconducting phase is simultaneously reduced in the present d-wave case. As is shown later, however, the MF-FOT appears only when $2T_{c0} > 10$, and hence, we focus here on this moderately clear region. One finds that, in this cleaner and d-wave pairing case, the combinations \hat{D}_s and \hat{E}_d are small enough to justify the neglect of the second term of eq.(8). For this reason, any contribution including the impurity-ladder vertex corrections will be neglected hereafter in the text and in Appendix A where our analysis using the coherent state for the LLs is explained.

We should note here that, strictly speaking, the eigenstates of the operator \hat{K}_2 in the $d_{x^2-y^2}$ -wave pairing are not the LLs, and that there are nonvanishing off-diagonal matrix elements between LLL and higher LLs with indices of multiples of four (i.e., $N = 4m$). However, in the range of Maki parameter considered in this paper, the instability line for the $N = 4$ LL modes, defined by $H_{c2}(0) = 0$ in our notation used below, lies far below $H_{c2}(T)$, and hence, we will neglect the off-diagonal elements in considering the $N = 0$ and 1 vortex states. Then, $w_{\mathbf{p}}$ in eq.(7) may be replaced by 1, and our analysis using the LL basis becomes straightforward. When $\psi_{\mathbf{r}_?}^{(N)}(\mathbf{q}_z)$ belongs to the N -th Landau level, the corresponding eigenvalue of \hat{K}_2 is given by

$$K_{2,N}(\mathbf{q}_z) = 2TN(0) \sum_{\mathbf{p}} \int_0^1 d\mathbf{p} \cdot \mathbf{p} L_N \left(\frac{\mathbf{p}^2}{2H} \right)^2 e^{-\frac{\mathbf{p}^2}{2H}} J_0 \left(2J \sin \left(\frac{\mathbf{q}_z s}{2} \right) \right); \quad (9)$$

where L_N is the N -th Laguerre function, J_0 is the zeroth Bessel function, and the function f is defined by

$$f(\mathbf{p}) = \frac{e^{-\mathbf{p}^2} \cos(2\mathbf{p} \cdot \mathbf{p})}{\sinh(2T)}; \quad (10)$$

The procedures leading to eq.(9) will be explained in Appendix A. After cutting the logarithmic divergence by its zero-field value, we obtain the final expression for the quadratic free energy.

$$F_2 = N(0) \sum_{\mathbf{q}_z} \sum_{\mathbf{r}_?} \psi_{\mathbf{r}_?}^\dagger(\mathbf{q}_z) \hat{K}_2(\mathbf{q}_z) \psi_{\mathbf{r}_?}(\mathbf{q}_z); \quad (11)$$

$$a_N(\mathbf{q}_z^2) = \ln(T/T_{c0}) + 2T \sum_{\mathbf{p}} \int_0^1 d\mathbf{p} \cdot \mathbf{p} (\sinh(2T))^{-1} f(\mathbf{p}) L_N \left(\frac{\mathbf{p}^2}{2H} \right)^2 e^{-\frac{\mathbf{p}^2}{2H}} J_0 \left(2J \sin \left(\frac{\mathbf{q}_z s}{2} \right) \right) \quad (12)$$

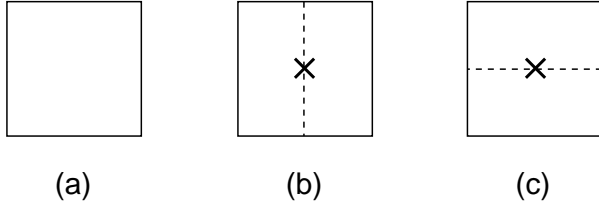


FIG. 1: Diagrams expressing the quartic term of the GL action

A possibility of an instability to an FFLO-like vortex solid in the N -th LL can be studied, at least near $H_{c2}(T)$ -line, by expanding ψ_N in powers of $Q = J \sin(qs/2)$ like

$$a_N(Q^2) = a_N(0) + a_N^{(1)} Q^2 + a_N^{(2)} Q^4 + \dots; \quad (13)$$

where

$$a_N^{(1)} = 2 T \int_0^{Z_1} d^2 f(\mathbf{r}) e^{-\frac{r^2}{2L_N^2}} L_N^2 \left(\frac{1}{2L_H}\right)^2; \quad (14)$$

and

$$a_N^{(2)} = \frac{T}{2} \int_0^{Z_1} d^4 f(\mathbf{r}) e^{-\frac{r^2}{2L_N^2}} L_N^2 \left(\frac{1}{2L_H}\right)^2; \quad (15)$$

As far as $a_N^{(2)} > 0$, the instability point to an FFLO solid state is determined by $a_N^{(1)} = 0$, and the corresponding transition is of second order.

QUARTIC TERM

The corresponding analysis for the higher order (quartic and 6th-order) terms of the GL functional is more complicated than that for the quadratic one. As already explained, the impurity-ladder vertex corrections will be neglected in the ensuing analysis of the nonlinear terms. Hereafter, it is convenient to work in a fixed Landau gauge $\mathbf{A} = (0; Hx; 0)$ and to represent the pair-field in terms of definite LL orbitals $u_{N,jk}(\mathbf{r})$

$$\psi_j(\mathbf{r}) = \frac{1}{S_H} \sum_{N,jk} u_{N,jk}(\mathbf{r}); \quad (16)$$

where $S_H = r_H L_y^{-1/2}$. In the present gauge, $u_{N,jk}(\mathbf{r})$ is given by

$$u_{N,jk}(\mathbf{r}) = \frac{1}{N!} e^{\frac{1}{2r_H^2} (x + kr_H^2)^2 +iky}; \quad (17)$$

where we introduce the creation and annihilation operators

$$\hat{c}^\dagger = \frac{r_H}{2} (x - iy) \quad (18)$$

for LLs.

For a moment, let us focus on a vortex solid within the LLL-subspace. An extension to the higher ($N = 1$) LL will be considered later. Then, the quartic term of the GL free energy functional can be written as

$$F_4 = \frac{1}{2} \sum_j \int d^2 \mathbf{r} \hat{K}_4 (f - ig) \psi_j(\mathbf{r}_1) \psi_j(\mathbf{r}_2) \psi_j(\mathbf{r}_3) \psi_j(\mathbf{r}_4) \quad (19)$$

$$= \sum_{j, \mathbf{r}_1, \mathbf{r}_2, \mathbf{r}_3, \mathbf{r}_4} \int d^2 \mathbf{r} \hat{K}_4 (f - ig) u_{0k_1j}(\mathbf{r}_1) u_{0k_2j}(\mathbf{r}_2) u_{0k_3j}(\mathbf{r}_3) u_{0k_4j}(\mathbf{r}_4) \quad (20)$$

where $\mathbf{r}_i = (r_i)$. In the impure case \hat{K}_4 consists of three terms represented in Fig. 1 and will be expressed as $\hat{K}_4 = \hat{K}_{4a} + \hat{K}_{4bc}$. The term \hat{K}_{4a} is given by

$$\hat{K}_{4a} = 2 T N(0) \sum_{\mathbf{F} \in S} \frac{\mathbf{j}_p \cdot \mathbf{j}}{(2i\mathbf{v} + \mathbf{v}_1)(2i\mathbf{v} + \mathbf{v}_2)(2i\mathbf{v} + \mathbf{v}_3)} + (2 \text{ } \S \text{ } 4) \quad (21)$$

$$= 2 T N(0) \sum_{i=1}^Z \int d^2 f(\mathbf{r}) \mathbf{j}_p \cdot \mathbf{j} e^{i(\mathbf{v}_1 \cdot \mathbf{r} + \mathbf{v}_2 \cdot \mathbf{r} + \mathbf{v}_3 \cdot \mathbf{r})} + (2 \text{ } \S \text{ } 4) \quad (22)$$

where the function f is defined by eq. (10), and the bracket $\int_{\mathbf{F} \in S}$ implies the angle-average over the Fermi surface. The sum of Fig. 1 (b) and (c), \hat{K}_{4bc} , is given by

$$\hat{K}_{4bc} = \frac{2 T}{N(0)} \sum_{\mathbf{F} \in S} \frac{\mathbf{j}_p \cdot \mathbf{j}}{(2i\mathbf{v} + \mathbf{v}_1)(2i\mathbf{v} + \mathbf{v}_2)} + \frac{\mathbf{j}_p \cdot \mathbf{j}}{(2i\mathbf{v} + \mathbf{v}_3)(2i\mathbf{v} + \mathbf{v}_4)} + (2 \text{ } \S \text{ } 4) \quad (23)$$

$$= \frac{2}{\pi} \frac{T}{N(0)} \sum_{i=1}^Z \sum_{j=1}^Y \sum_{k=1}^X \sum_{l=1}^D \int_{F:S} d_{if} \left(\frac{X^4}{4} \right) \int_{F:S} d_{if} \left(\frac{X^4}{4} \right) e^{i(\nu_1 + \nu_2 + \nu_3 + \nu_4)} \int_{F:S} d_{if} \left(\frac{X^4}{4} \right) e^{i(\nu_1 + \nu_2 + \nu_3 + \nu_4)} + \left(\frac{2}{\pi} \frac{T}{N(0)} \right) (24)$$

The following results which are derived in the appendix are quite convenient.

$$e^{i\nu} u_{0jk}(r_?) = e^{\frac{(j^2 - k^2)}{4}} e^{\frac{1}{2}(x=r_H + k r_H + \dots)^2 + i k y} ; \quad (25)$$

$$e^{i\nu} u_{0jk}(r_?) = e^{\frac{(j^2 - k^2)}{4}} e^{\frac{1}{2}(x=r_H + k r_H + \dots)^2 - i k y} ; \quad (26)$$

where $\nu = \nu_H$ and $\nu = \nu_x + i\nu_y$ is the complex coordinate specifying the position $p = p_F \hat{p}$ on the Fermi surface. With this identity and eq.(57), we obtain the following results.

$$\sum_{i=1}^Z d^2 r_? \hat{K}_{4a}(f_{ig}) u_{0k_1j}(r_{?1}) u_{0k_2j}(r_{?2}) u_{0k_3j}(r_{?3}) u_{0k_4j}(r_{?4}) \quad (27)$$

$$= \frac{2}{\pi} \frac{T N(0)}{2 S_H} \sum_{i=1}^Z \sum_{j=1}^Y \sum_{k=1}^X \sum_{l=1}^D (Re^2)^4 e^{i(\nu_1 + \nu_2 + \nu_3 + \nu_4)} u_{0k_1j}(r_{?1}) u_{0k_2j}(r_{?2}) u_{0k_3j}(r_{?3}) u_{0k_4j}(r_{?4}) \quad (28)$$

$$\sum_{i=1}^Z d^2 r_? \hat{K}_{4bc}(f_{ig}) u_{0k_1j}(r_{?1}) u_{0k_2j}(r_{?2}) u_{0k_3j}(r_{?3}) u_{0k_4j}(r_{?4}) \quad (29)$$

$$= \frac{2}{\pi} \frac{T N(0)}{2 S_H} \sum_{i=1}^Z \sum_{j=1}^Y \sum_{k=1}^X \sum_{l=1}^D (Re^2)^2 e^{i(\nu_1 + \nu_2 + \nu_3 + \nu_4)} u_{0k_1j}(r_{?1}) u_{0k_2j}(r_{?2}) \quad (30)$$

where the orbital-depairing weight function for the quartic term is given by

$$I_4(f_{ig}) = e^{\frac{1}{4} \sum_{i=1}^4 j_i^2 + \frac{1}{2} \left(\frac{1}{13} + \frac{1}{24} \right) + (1 + \frac{1}{3})(2 + \frac{1}{4}) + 2 \Gamma_H(k_{13} \frac{1}{13} k_{24} \frac{1}{24})} ; \quad (31)$$

where $k_{ij} = k_i - k_j$. Finally we have a quartic term

$$F_4 = \frac{N(0)}{2} \frac{X}{2 S_H} \sum_{j=fk_1g}^{k_1+k_3, k_2+k_4} V_4(fk_1g) e^{\frac{x_H^2}{4} (k_{13}^2 + k_{24}^2)} k_{1;j} k_{2;j} k_{3;j} k_{4;j} ; \quad (32)$$

$$V_4(fk_1g) = \frac{2}{\pi} \frac{T}{N(0)} \sum_{i=1}^Z \sum_{j=1}^Y \sum_{k=1}^X \sum_{l=1}^D (Re^2)^4 I_4(f_{ig}) \quad (33)$$

Later, we will comment on the fact that, consistently with the neglect of the second term in eq.(8), the second line of eq.(33) arising from \hat{K}_{4bc} is safely negligible compared with the first \hat{K}_{4a} term in the relatively clean case with $2 T_{c0} > 10$ of our interest.

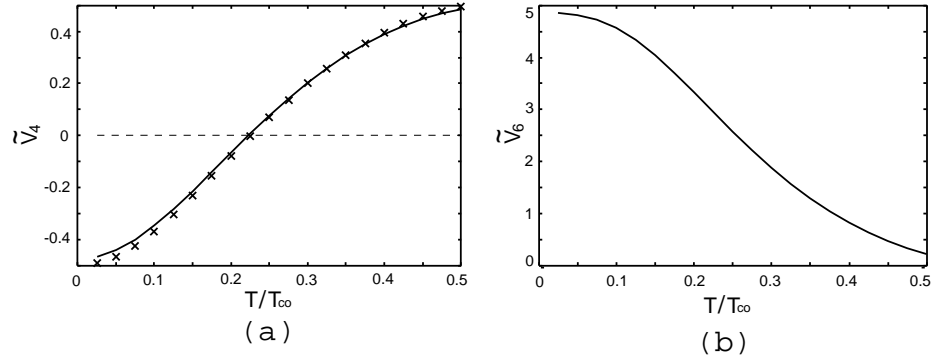


FIG. 3: Numerical results of the dimensionless coefficients (a) $V_4 = V_4(fk_j = 0g) = \frac{2}{H}$ and (b) $V_6 = V_6(fk_j = 0g) = \frac{4}{H}$ on the H_{c2} -curve at lower temperatures $T < 0.5T_{c0}$. The value $\mu_0 H_{c2}^{orb} = 2 k_B T_{c0} = 0.8$ and $(2 T_{c0})^{-1} = 0.05$ was commonly used. In (a), the cross symbols represent the result due only to $g_1(a)$.

where V_{6a} is given by

$$V_6(fk_j g) = \sum_{i=1}^Z \sum_{j=1}^Y \sum_{k=1}^X \left(\frac{D}{8(\text{Re } e^2)^6} I_6(f_i g_j) j_{6=0; 166=1} = H \right) + \left(\frac{D}{8(\text{Re } e^2)^6} I_6(f_i g_j) j_{6=0; 1;5=1;5} = H ; 3=3 = H ; 2;4=(2;4+3) = H \right) \quad (41)$$

In deriving the MF phase diagram and its impurity dependence, we will use an additional approximation below. As mentioned in x1, the orbital depairing effect arising from the gauge invariant gradients ∇_j , in low T limit, have to be incorporated nonperturbatively. Consequently, additional dependences on k_{ij} appear in V_4 and V_6 , while the gaussian factors on k_{ij} in F_4 and F_6 are direct consequences of restricting the pair-field into the LLL subspace and also appear in the familiar GL expression with spatially local nonlinear terms. That is, the k_{ij} dependences in V_4 and V_6 can be seen as spatially nonlocal contributions to the nonlinear terms and affect the structure of vortex solid. Actually, in LLL and the case with no paramagnetic depairing, this nonlocality in the quartic GL term results in the structural transition of vortex solid between the rhombic and square lattices [21]. However, an energy difference affecting the lattice structure is extremely small reflecting a small difference of the Abrikosov factor (denoted as κ_A and κ_A below), and, at least as far as the SC transition in the MF approximation at H_{c2} is concerned, such nonlocal contributions are safely negligible. For this reason, the k_{ij} 's in V_4 and V_6 will be replaced hereafter by zero. Then, the GL model derived microscopically takes the form

$$F_{loc} = N(0) \sum_{\mathbf{r}_2} d^2 \mathbf{r}_2 \sum_{\mathbf{q}_z} \left(a_0 (\alpha_z^2) j_{\mathbf{q}_z}^{(0)} (\mathbf{r}_2) j_{\mathbf{q}_z}^2 + \sum_j \left(\frac{V_4(fk_j g = 0)}{2} j_j^4 + \frac{V_6(fk_j g = 0)}{3} j_j^6 \right) \right) \quad (42)$$

Temperature variations of the coefficients $V_4(fk_j g = 0)$ and $V_6(fk_j g = 0)$ calculated along the $H_{c2}(T)$ -curve are shown, respectively, in Fig.3 (a) and (b). To clarify that the contributions of Fig.1 (b) and (c) are safely negligible, V_4 in Fig.3 (a) was calculated in terms of $(2 T_{c0})^{-1} = 0.05$, the value used in Fig.4 (b) below. The coefficient V_4 is negative at lower temperatures, while V_6 is positive over a broad region so that the GL expression (42) is well-defined.

MEAN FIELD PHASE DIAGRAM

Below, the MF phase diagram will be examined based on the functional, eq.(42). First, let us neglect a possibility of an FFLO-like state and assume the uniform vortex solid independent of j as the MF solution. Then, the first term in the bracket of eq.(42) is replaced by $\sum_j a_0(0) j_j^2$, and the MF solution is obtained in a standard way. The character of the MF transition at $H_{c2}(T)$ -line changes with increasing field from the second order one to a discontinuous one at a temperature T^* where the coefficient V_4 of the quartic term becomes negative, reflecting that the spin depairing is more effective upon

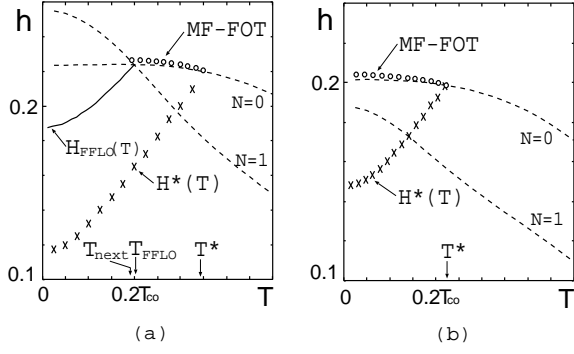


FIG. 4: MF phase diagrams in (a) clean limit $((2T_{c0})^{-1} = 0)$ and (b) the moderately clean case $((2T_{c0})^{-1} = 0.05)$.

cooling and with increasing H . To obtain MF results in $T < T^*$, higher nonlinear terms are necessary in the GL expression. As already seen, the coefficient V_6 ($fk_i = 0g$) is positive over a broad temperature range, and thus, the expression eq.(42) terminated at the 6th order term will be sufficient for our purpose. Further, let us introduce the effective coefficients $\tilde{B} = V_4$ ($fk_i = 0g$) of the quartic term and $\tilde{c} = V_6$ ($fk_i = 0g$) of the 6th order term, respectively, where

$$\begin{aligned} \tilde{B} &= \frac{j_j(x_j)j_j^4}{(nj_jj_i)^2}; \\ \tilde{c} &= \frac{j_j(x_j)j_j^6}{(nj_jj_i)^3}; \end{aligned} \quad (43)$$

Then, the following MF results in $T < T^*$ are found. First, the MF transition point in $T < T^*$ and in LLL is determined by

$$a_0(0) = a_{0;c} \frac{3\tilde{B}^2}{16\tilde{c}}; \quad (44)$$

while the supercooling (superheating) point is given by $a_0(0) = 0$ ($a_0(0) = \tilde{B}^2/(4\tilde{c})$). Next, the energy barrier U_{barr} between the $j_j = 0$ solution and the jump value of j_j at the transition, $j_{j;c} = \sqrt{3\tilde{B}/4\tilde{c}}$, is given by

$$U_{\text{barr}} = N(0) \frac{\tilde{B}j_j^3}{48\tilde{c}^2}; \quad (45)$$

Further, by calculating the mean squared amplitude j_j^2 of the Gaussian fluctuation when $a_0(0) = a_{0;c}$ and in 2D limit, one also finds

$$j_j^2 \sim \frac{T_{c2} j_{j;c}^2}{U_{\text{barr}}}; \quad (46)$$

where T_{c2} is the transition temperature. Thus, the fluctuation strength is enhanced with decreasing \tilde{B} and increasing \tilde{c} and, as expected, is measured at T_{c2} by the inverse of the energy barrier. Hence, if this MF-FOT occurs as a true FOT in real systems, a clear hysteresis is expected in a system with weaker fluctuation.

However, in higher fields and lower temperatures where the spin depairing becomes more important, an FFLO-like helical vortex solid may become more favorable. As far as the width $a_{0;c}$ is sufficiently small, the gradient terms have only to be incorporated in the lowest order terms in j_j . That is, this structural transition line $H_{\text{FFLO}}(T)$ between the FFLO-like solid and the uniform vortex solid may be discussed within the coefficient $a_0(q_z^2)$. Actually, according to the calculation results of V_4 and V_6 in Fig.3, $a_{0;c}$ in Fig.4 is at most of the order of 10^{-2} . Assuming, e.g., a solution $\sim q_z e^{iz}$ with a uniform current along the field, a second order structural transition line $H_{\text{FFLO}}(T)$ is obtained according to eq.(13) as the position $a_0^{(1)} = 0$ if $a_0^{(2)} > 0$ there. We have verified that $a_0^{(2)}$ is always positive along the $H_{\text{FFLO}}(T)$ -line and increases upon cooling at a fixed field above $H_{\text{FFLO}}(T)$. Further, since the paramagnetic depairing effect is enhanced with increasing field and decreasing temperature, as the example in Fig.4 shows, a possible $H_{\text{FFLO}}(T)$ -curve should decrease upon cooling.

The MF phase diagrams following from the GL coefficients derived above are shown in Fig.4 for two different impurity strengths ($(2T_{c0})^{-1}$ -values). The used value of paramagnetic parameter $\mu_0 H_{c2}^{\text{orb}} = 2T_{c0}$, corresponding to the Maki parameter, is 0.8, where $H_{c2}^{\text{orb}} = 0.56 \mu_0 = (2T_{c0})$ is the 2D orbital limiting field at $T = 0$ in pure case, and $\mu_0 = v_F = 2T_{c0}$. The field values in the figures were normalized by H_{c2}^{orb} . The curve $H(T)$ indicated by the cross symbols is defined by the condition $V_4 = 0$ and cannot be directly seen in experiments. The coefficient V_4 is positive in $H < H(T)$ (see Fig.3 (a)). In contrast, the portion (open circles) in $T < T^*$ of $H_{c2}(T)$ on which the MF-SC transition becomes discontinuous is experimentally measurable together with the second order transition line $H_{\text{FFLO}}(T)$ (solid curve) to the FFLO vortex solid. In the temperature regions where the MF-FOT does not occur, the dashed curves indicated by $N = 0$ or $N = 1$ become the $H_{c2}(T)$ -line, on which $a_0(0)$ or $a_1(0) = 0$, and a second order MF transition occurs there.

It will be important to, in relation to real phase diagrams of related materials, understand how the $H_{\text{FFLO}}(T)$ curve and the characteristic temperatures are affected by the impurity strength. By comparing both figures with each other, the region $H_{\text{FFLO}}(T) < H < H_{c2}(T)$ is found to be easily lost by a slight increase of impurity strength $(2T_{c0})^{-1}$. In contrast, the onset T^* of the MF-FOT behavior is relatively insensitive to the sample purity. Nevertheless, when $(2T_{c0})^{-1}$ goes beyond 0.095 while $\mu_0 H_{c2}^{\text{orb}} = 2T_{c0} = 0.8$ was kept, the MF-FOT region at $H_{c2}(T)$ is also lost, and the MF transition at $H_{c2}(T)$ is continuous at all temperatures. This result is contrast to other works [6, 13] in which the presence of a MF-FOT was argued under the use of dirty limit. We find that, instead, the FOT obtained in the dirty

limit [13] never occurs in $T \rightarrow 0$ limit when $E_F > 1$ under which the usual dirty limit may be valid. On the other hand, the results in ref.[6] are derived by completely neglecting the orbital depairing and are not comparable with the present ones. Further, we stress that, in contrast to results in previous works [12] taking account of both the orbital and spin depairing effects, the results in Fig.4 imply that always $T > T_{\text{FFLO}}$. Thus, if the MF transition at H_{c2} truly occur as a genuine transition, a strong FOT should have been observed in superconductors with strong Pauli paramagnetic depairing effect. This point will be discussed in x4 in relation to real materials.

Since, as already mentioned, the width $a_{0,c}$ is unexpectedly small, the MF-FOT in Fig.4 may be regarded as being relatively weak. However, it does not mean a strong fluctuation. Actually, in system with a large $N(0)$ in zero field such as CeCoIn_5 , the fluctuation strength $T = U_{\text{barr}}$ itself becomes extremely small in the low T region of our interest.

In $T < T_{\text{next}}$, the $H_{c2}(T)$ line and hence, the vortex lattice itself just below it are determined by the next lowest ($N = 1$) LL. Thus, a competition between the FFLO-like solid within LLL and the solid within the $N = 1$ LL has to be examined just above the $H_{\text{FFLO}}(T)$ line. Since this is an issue of a transition between vortex lattice structures defined within the planes perpendicular to the field, a detailed description of the stable vortex lattices in d-wave pairing cases is required to address this. As already mentioned, however, the nonlocality of the nonlinear terms affecting the in-plane lattice structure was neglected in this paper. We will postpone a study of structural transitions to higher LL solids in $H > H_{\text{FFLO}}$ to our future study.

SIMULATION RESULTS

In this section, we explain our results on Monte Carlo simulations for the model eq.(42). Their preliminary version and the corresponding results in its extension to the multilayered case were reported in ref.[22] and [10], respectively. Below, the size dependence for 2D case and results for the case with weaker fluctuation are presented together with those for a one-dimensional Gln model with no phase transition.

The partition function we examine is

$$Z = \text{Tr} \exp(-F); \quad (47)$$

where the functional $F = F_{\text{loc}} = k_B T$ is rewritten as

$$F = \int d^2r \left[\frac{1}{2} |\psi|^2 + \frac{1}{2} \psi^2 + \frac{1}{3} \psi^3 + \frac{1}{4} \psi^4 + \frac{1}{5} \psi^5 + \frac{1}{6} \psi^6 \right]; \quad (48)$$

where $\psi(r)$ is the order parameter field defined within

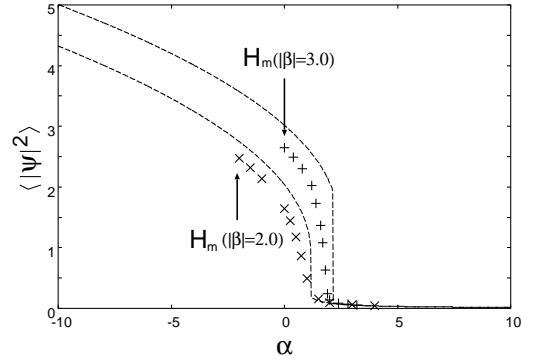


FIG. 5: Numerical data (symbols) of $\langle |\psi|^2 \rangle$ -dependence (i.e., H -dependence) of $\langle |\psi|^2 \rangle$ in 2D case. The system size (6,4), and the j values 2.0, 3.0 were used. The dashed curves denote the corresponding results in the Hartree approximation in which no phase transition occurs.

LLL, and

$$\begin{aligned} &= \frac{r_H^2 N(0)}{k_B T} \frac{2=3}{V_6^{1=3}} \frac{a_0}{V_6^{1=3}}, \quad 0 \leq \frac{H}{H_0} \leq 1; \\ j &= \frac{r_H^2 N(0)}{k_B T} \frac{1=3}{V_6^{2=3}} \frac{j_4 j}{V_6^{2=3}}; \end{aligned} \quad (49)$$

where H_0 denotes H_{c2} in the case with no MF-FOT. Since, as mentioned earlier, $a_{0,c}$ measuring the difference $(H_{c2} - H_0) = H_0$ is quite small in the parameter values used in this paper, H_0 will not be distinguished from H_{c2} below. Note that, except a numerical factor, j is identical with $U_{\text{barr}} = k_B T$. Thus, the T -dependent parameter j measures the fluctuation strength, and a change of temperature can be represented as a change only of j if the magnetic field variable is appropriately rescaled.

Our simulation method closely follows that used in the simulations [23, 24] for the case with a positive quartic term in place of j in eq.(48). The order parameter field is expanded in terms of the LLL basis function $\psi_n(x; y)$ consistent with a quasi-periodic boundary condition [23] as $\psi = \sum_n c_n \psi_n(x; y)$, and the system sizes L_x and L_y of a rectangular cell satisfy the commensurability with a triangular lattice ground state through the relation $L_x = L_y = \sqrt{3} N_x = 2 N_y$ (As mentioned earlier, due to the neglect of nonlocality in the GL nonlinear terms, the ground state in the present case is a triangular lattice although the pairing state is a four-fold d-wave one). The Markov chains for c_n are generated by the Metropolis algorithm. The system sizes we have studied were $(N_x, N_y) = (6, 4)$ and $(8, 6)$. We used 5×10^6 MC steps for thermalization which was further verified in terms of another 1×10^6 MC steps. Further, regarding the microscopic details, the same parameter values as in Fig.3 and 4 were used.

First, let us present and explain 2D simulation results. To study fluctuation effects on the MF-FOT, the mean-

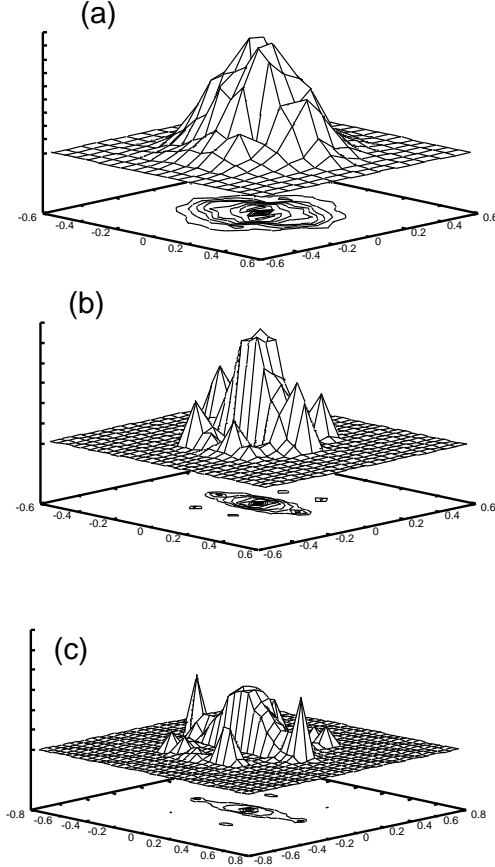


FIG. 6: $S(q)$ data for $j = 2$ corresponding to Fig.5 at (a) $\beta = 0.75$ and (b) 2.0 . (c) $S(q)$ at $\beta = 2.0$ for larger system size $(8, 6)$.

squared average of the pair-field $\langle j^2 \rangle$ was calculated. It corresponds to the magnetization when a_0 is the measure, primarily, of H . Hence, if it shows not a true jump (insensitive to the system size) but a rounded behavior near H_{c2} , a genuine FOT at H_{c2} is judged to be absent. Further, as a measure of the vortex-positional ordering (vortex-solidification) presumably occurring below H_{c2} in 2D and 3D, we have examined the structure factor $S(k)$ defined [25] as the Fourier transform of the correlation function of $j(r)$.

Results are shown in Fig.5 and 6 and essentially the same as those in the layered case [10]. As is clear from the $j = 2$ data of Fig.5, the discontinuous jump of $\langle j^2 \rangle$ at H_{c2} in the MF approximation is rounded due to the fluctuation, and thus, no genuine FOT has occurred at H_{c2} . We note that the coefficient $\beta_0(T)$ is beyond 50 in the temperature assumed there. If the abscissa in Fig.5 is expressed by the reduced field $(H - H_0)/H_0$, even the rounded behavior of $\langle j^2 \rangle$ for $j = 2$ cannot be distinguished from a strictly sharp discontinuity. As the corresponding $S(k)$ results in Fig.6 show, the vortex solidification point lies just below H_{c2} . Further, through the size dependence of $S(k)$ data illustrated in Fig.6 (b)

and (c), the solidification is found to be enhanced by the boundary condition in a smaller system (b)). It will be clear that the six-fold symmetry of Bragg peaks is more remarkable in (b). This will be sufficient for justifying our expectation that the solidification occurs below H_{c2} .

Next, we report on consequences of an extension of simulation for the layered system [10] composed of four layers to weaker fluctuation cases with $j > 3.0$. In our simulation for the layered case, we used 1.5×10^6 MC steps for thermalization and another 2×10^6 MC steps for further observation, and we used the lateral boundary condition $L_x = L_y = 2N_x = 3N_y$ with $(N_x; N_y) = (6; 6)$. As the numerical data in Fig.7 show, a hysteresis suggesting a genuine FOT appears in $\langle j^2 \rangle$ curves in the vicinity of H_{c2} for $j > 3$. As mentioned below eq.(49), however, setting a larger j -value corresponds to simulating the same (original) GL model eq.(42), with fixed values of GL coefficients a_0 , V_4 , and V_6 , at a lower T -value, and hence, this hysteresis is not an evidence of a genuine FOT at finite T . Actually, the data in Fig.7 suggest that the system, at least in the vicinity of H_{c2} , has not reached the thermodynamic equilibrium even during

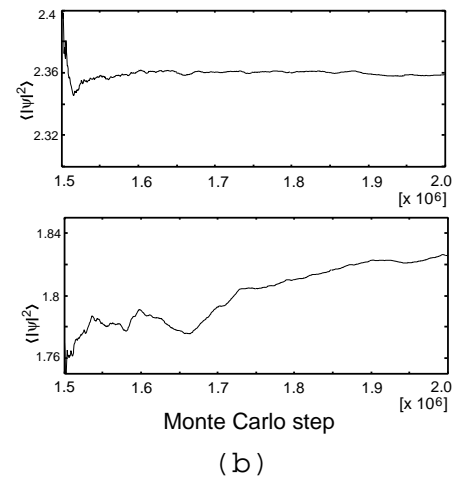
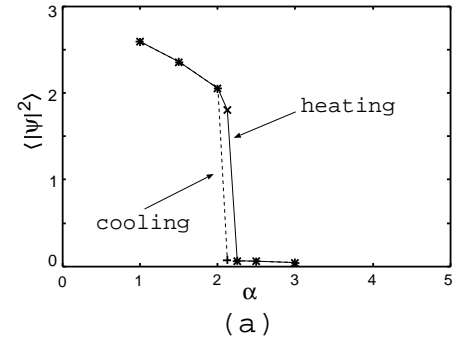


FIG. 7: (a) Numerical data, similar to Fig.5, for $j = 3.5$. (b) The history of $\langle j^2 \rangle$ for heating process at $\beta = 1.5$ (upper panel) and $\beta = 2.125$ (lower panel). Note the large time variation of $\langle j^2 \rangle$ when $\beta = 2.125$.

the MC steps we have observed. Below, we show in Fig.8 that a similar hysteresis suggestive of a genuine FOT occurs in a more familiar model with no phase transition at finite T , i.e., a 1D GL model expressed by

$$F_{1d} = \int dx \left[a j(x)^2 + c \frac{d j(x)}{dx}^2 + \frac{b j(x)^4}{2} + \frac{1}{3} j(x)^6 \right]; \quad (50)$$

where j is a function only of x . This 1D model is used here for comparison because the fluctuation in 3D GL model within LLL is expected to be similar to the corresponding 1D GL model in zero field. We chosen the values $b j = 5.0$ and $c = 4.0$. Due to the smaller degrees of freedom in the superconducting fluctuation in the 1D case, the relaxation to the thermal equilibrium (i.e., a disappearance of hysteresis), as Fig.8 (b) shows, manages to be reached within the practically possible MC steps. It is quite difficult to verify the corresponding relaxation of the present layered system expressed by eq.(48) within practically possible MC steps because of extremely many degrees of freedom of the quasi 2D superconductors in nonzero field. Nevertheless, when combining this result with the simulation results in $j j = 3$ and the purely theoretical argument [10], it is clearly reasonable to argue the absence of true FOT at H_{c2} at any finite T .

DISCUSSION

As explained in Introduction, the present work was originally motivated as an extension of the problem of vortex phase diagram to the more general cases with spin (paramagnetic) depairing. Since the absence of MF second order transition at H_{c2} in lower fields is well-established, it is unreasonable to expect the MF-FOT at H_{c2} resulting from the Pauli paramagnetic depairing in higher fields to truly occur as a genuine FOT. The recent finding of the FOT-like nearly discontinuous crossover at H_{c2} in the heavy fermion superconductor $CeCoIn_5$ provides us for a good occasion of a close comparison between the present theory and real data. Further, recent data showing a small hysteresis in heat capacity and suggesting a second order transition between the FFLO-like vortex solid and the ordinary vortex solid stimulate necessity of detailed theoretical studies of vortex phase diagram in the Pauli-limited region.

One might wonder why we think a small hysteresis seen in specific heat measurements of ref.[14] is consistent with the present theory [10] arguing the absence of a genuine FOT at H_{c2} . As explained in the last section, a hysteresis arising from an incomplete relaxation at long but finite time scales arises even in numerical experiments at low enough T for a system in which a MF-FOT cannot occur as a true FOT. Since the theoretical reasoning [10] of the absence of the transition at H_{c2} is valid irrespective of the sign of the quartic term of the GL func-

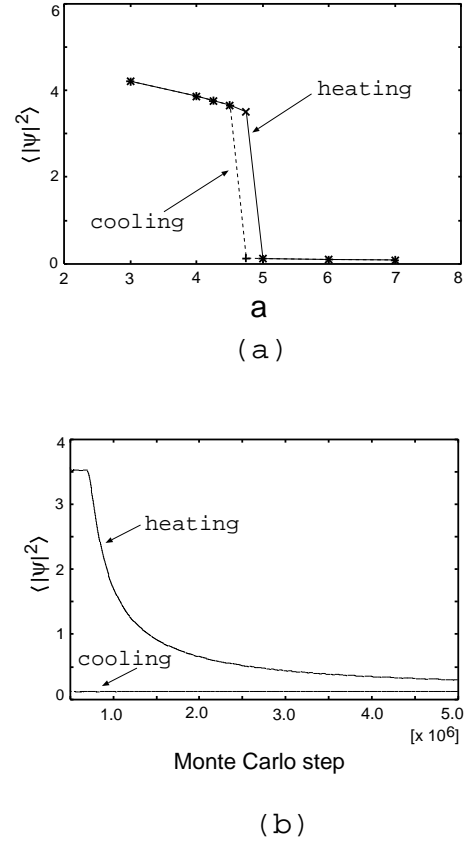


FIG. 8: (a) Data similar to Fig.7 (a) for the 1D GL model, eq.(50). (b) Data showing a recovery of thermal equilibrium after many MC steps.

tional, we strongly believe this to be a valid explanation on the observed hysteresis [14] accompanying the FOT-like behavior. Actually, the onset of hysteresis in ref.[14] lies slightly above the temperature T_{FFLO} at which FFLO transition line branches from the MF-FOT (i.e., $H_{c2}(T)$) line and thus, does not seem to correspond to another phase boundary separating a true FOT from the nearly FOT behavior at higher temperatures with no hysteresis [17].

What we wish to stress within the MF approximation is that, in bulk systems with orbital depairing effect, the FFLO onset temperature T_{FFLO} lies much below the onset of the discontinuous MF transition at H_{c2} and that, depending on the purity of the sample, the temperature and field region of the FFLO-like solid easily shrinks. This result that the FFLO region is rarely seen compared with the nearly discontinuous crossover at H_{c2} is opposite to those in previous works [12], where the orbital depairing was treated only perturbatively, and is a new theoretical result consistent with the data in $CeCoIn_5$.

Finally, let us point out that the present theory easily explains why the transition to an FFLO-like phase and the nearly discontinuous crossover at H_{c2} implying the MF-FOT were measured not in organic materials with

larger anisotropy but in a heavy fermion material with weaker anisotropy. At least at the MF level, the case with a field parallel to the layers in more anisotropic materials has weaker orbital depairing effects and is the best candidate for observing Pauli-limited phenomena such as the FFLO state and the MF-FOT. The organic materials satisfy this requirement, and actually, the observed upwardly increasing $H_{c2}(T)$ curve determined resistively [26] under high fields parallel to the layers implies a large Maki parameter and is an evidence that the spin depairing is microscopically important without being disturbed by the impurity effect. However, both the FFLO-transition and the MF-FOT have not been seen in the organic materials. Although the heavy fermion material CeCoIn₅ with a much weaker anisotropy has no such upward $H_{c2}(T)$ -curve presumably as a result of a relatively weaker spin depairing effect, one might wonder why both the transition behaviors due to the spin depairing have occurred in this material. This puzzling facts are easily resolved by taking account of fluctuation effects examined in this paper. Typically, in the organic and cuprate materials [26, 27], the fluctuation effect is much stronger compared with those of CeCoIn₅. Actually, a shorter coherence length tends to result in a larger Maki parameter and to enhance the fluctuation even in the parallel field case [7, 28]. Consequently, as shown in x3, the MF-FOT behavior is rounded and becomes merely a continuous crossover as a result of the absence of the true FOT at H_{c2} . Further, a remarkable field and temperature range of the vortex liquid region in which the resistance is finite may be created below $H_{c2}(T)$ -curve even in the parallel field case [28] where the fluctuation effect is minimized. Since the FFLO phase is limited to a narrow field range below H_{c2} , and the modulation parallel to the field does not lead to any ordering in the vortex liquid, the vortex liquid region should mask and erase the FFLO phase in a strongly fluctuating superconductor. For these reasons, cleaner superconducting materials with weaker fluctuation such as CeCoIn₅ are the best candidates for examining the MF high field phase diagram in the case with Pauli-limiting effect.

APPENDIX A : DERIVATION OF \hat{K}_2

In this appendix we present how to solve the eigenvalue problem of \hat{K}_2 or equivalently of \hat{D}^\dagger . Using the identity $1 = \int_0^\infty d\epsilon e^{-\epsilon}$ and after the energy integration, we get the differential operator of infinite order

$$\hat{D}^\dagger(2'') = \sum_{n \geq 0} \sum_{l \geq 0} d e^{(2''+1-\epsilon)} J_0(2J \sin(\frac{q_z s}{2}))$$

$$\cos(2I_0) \int_{F.S.} d\mathbf{r} e^{i\mathbf{v} \cdot \mathbf{r}} = \cos(2I_0) \int_{F.S.} d\mathbf{r} e^{i\mathbf{v} \cdot \mathbf{r}}; \quad (51)$$

where J_0 is the 0-th Bessel function. Expanding the exponential and averaging on the Fermi surface, the last part of the above equation becomes

$$\int_{F.S.} d\mathbf{r} e^{i\mathbf{v} \cdot \mathbf{r}} = e^{-(\frac{v}{2})^2 X} \frac{2 \frac{v^2}{2}}{(m!)^2} \hat{\Lambda}_+^m \hat{\Lambda}_+^m + \text{off diagonal terms}; \quad (52)$$

where $\hat{\Lambda}_\pm$ are given below the eq. (17), and an circular Fermi surface was assumed. As explained above eq.(9), we are interested in the diagonal terms. Noticing the eigenvalue of $\hat{\Lambda}_+^m \hat{\Lambda}_+^m$ in the N -th Landau level is $\frac{N!}{(N-m)!}$ and performing the m -summation, we obtain eq. (9).

APPENDIX B : EXPRESSIONS OF I_4 AND I_6

In this appendix we study the function $e^{i\mathbf{v} \cdot \mathbf{u}_{0;k}(\mathbf{r}_?)}$ and derive the expressions of I_4 and I_6 . If we denote the position on a (2-dimensional) Fermi surface by a complex number $v_F = v_F(\cos\theta + i\sin\theta)$ and define $\mathbf{r}_? = \mathbf{r}_H + \mathbf{r}_?$, we have

$$e^{i\mathbf{v} \cdot \mathbf{u}_{0;k}(\mathbf{r}_?)} = e^{\frac{i}{2}(\hat{\Lambda}_+ + \hat{\Lambda}_-)} = e^{\frac{i}{4}(\hat{\Lambda}_+^2 + \hat{\Lambda}_-^2)} e^{\frac{i}{2}(\hat{\Lambda}_+ + \hat{\Lambda}_-)}; \quad (53)$$

where we used the operator identity $e^{\hat{A} + \hat{B}} = e^{\frac{1}{2}[\hat{A}, \hat{B}]} e^{\hat{A}} e^{\hat{B}}$ if $[\hat{A}, \hat{B}]$ is a classical number. From this expression it is sufficient to know the form of $e^{\frac{i}{2}(\hat{\Lambda}_+ + \hat{\Lambda}_-)} u_{0;k}(\mathbf{r}_?)$. Using the above identity to obtain

$$e^{\frac{i}{2}(\hat{\Lambda}_+ + \hat{\Lambda}_-)} = e^{\frac{i}{8}(\hat{\Lambda}_+^2 + \hat{\Lambda}_-^2)} e^{i\mathbf{r}_H \cdot \mathbf{q}_y} e^{i\mathbf{r}_H \cdot \mathbf{q}_x}; \quad (54)$$

and noticing $e^{i\mathbf{q} \cdot \mathbf{g}(\mathbf{x})} = g(\mathbf{x} + \mathbf{g})$ for any non-singular function $g(\mathbf{x})$, we finally have

$$e^{i\mathbf{v} \cdot \mathbf{u}_{0;k}(\mathbf{r}_?)} = e^{\frac{i}{4}(j^2 - 2)} e^{\frac{i}{2}(\mathbf{x} = \mathbf{r}_H + \mathbf{k} \mathbf{r}_H)^2 + i\mathbf{k} \cdot \mathbf{y}}; \quad (55)$$

$$e^{i\mathbf{v} \cdot \mathbf{u}_{0;k}(\mathbf{r}_?)} = e^{\frac{i}{4}(j^2 - 2)} e^{\frac{i}{2}(\mathbf{x} = \mathbf{r}_H + \mathbf{k} \mathbf{r}_H)^2 + i\mathbf{k} \cdot \mathbf{y}}; \quad (56)$$

With the help of the above identities, the following results are easily derived.

$$\begin{aligned}
 & \sum \frac{d^2 r_i}{S_H} e^{i(\nu_1 + \nu_2 + \nu_3 + \nu_4)} u_{0;k_1}(r_1) u_{0;k_2}(r_2) u_{0;k_3}(r_3) u_{0;k_4}(r_4) \\
 &= \frac{r}{2} \frac{h_P}{k_1 + k_3; k_2 + k_4} e^{\frac{r_H^2}{4}(k_{13}^2 + k_{24}^2)} e^{\frac{1}{4} \sum_{i=1}^4 j_i^2 + \frac{1}{2}(\nu_1^2 + \nu_2^2) + (\nu_1 + \nu_3)(\nu_2 + \nu_4) + 2r_H(k_{13} - k_{24})} \\
 & \frac{r}{2} \frac{h_P}{k_1 + k_3; k_2 + k_4} e^{\frac{r_H^2}{4}(k_{13}^2 + k_{24}^2)} I_4(f, ig)
 \end{aligned} \quad (57)$$

$$\begin{aligned}
 & \sum \frac{d^2 r_i}{S_H} e^{i(\nu_{\text{odd}} + \nu_i + \nu_{\text{even}})} u_{0;k_1}(r_1) u_{0;k_2}(r_2) u_{0;k_3}(r_3) u_{0;k_4}(r_4) u_{0;k_5}(r_5) u_{0;k_6}(r_6) \\
 &= \frac{r}{3} \frac{h_P}{K_{\text{odd}}; K_{\text{even}}} e^{\frac{r_H^2}{6} \sum_{(i,j)} k_{ij}^2} \\
 & \frac{r}{3} \frac{h_P}{K_{\text{odd}}; K_{\text{even}}} e^{\frac{r_H^2}{6} \sum_{(i,j)} k_{ij}^2} I_6(f, ig)
 \end{aligned} \quad (58)$$

where $K_{\text{odd}} = k_1 + k_3 + k_5$; $K_{\text{even}} = k_2 + k_4 + k_6$ and $(i; j) = f(1;3); (3;5); (5;1); (2;4); (4;6); (6;2)g$.

REFERENCES

-
- [1] A. M. Clogston, Phys. Rev. Lett. 9, 266 (1962).
 [2] K. Maki and T. Tsuneto, Prog. Theor. Phys. 31, 945 (1964).
 [3] T. Suzuki et al, J. Phys. Soc. Jpn. 69, 1462 (2000).
 [4] P. Fulde and R. A. Ferrell, Phys. Rev. 135, A 550 (1964).
 [5] A. I. Larkin and Y. N. Ovchinnikov, Sov. Phys. JETP 20, 762 (1965).
 [6] D. F. Agterberg and K. Yang, J. Phys. Condens. Matter 13, 9259 (2001).
 [7] R. Ikeda and K. Isotani, J. Phys. Soc. Jpn. 67, 983 (1998).
 [8] For instance, see T. Nattermann and A. Sheidl, Adv. Phys. 49, 607 (2000).
 [9] R. Ikeda, J. Phys. Soc. Jpn. 70, 219 (2001).
 [10] H. Adachi, S. Koikegami, and R. Ikeda, cond-mat/0303540.
 [11] L. W. G. Gunther and L. G. Unther, Phys. Rev. Lett. 16, 966 (1966).
 [12] M. Houzet and A. Buzdin, Phys. Rev. B 63, 184521 (2001).
 [13] K. Maki, Phys. Rev. 148, 362 (1966).
 [14] A. Bianchi et al, cond-mat/0304420.
 [15] K. Izawa et al, Phys. Rev. Lett. 87, 057002 (2001).
 [16] T. Tayama et al, Phys. Rev. B 65, 180504 (2002).
 [17] A. Bianchi et al, Phys. Rev. Lett. 89, 137002 (2002).
 [18] T. P. Murphy et al, Phys. Rev. B 65, 100514 (2002).
 [19] R. A. Klemm et al, Phys. Rev. B 12, 877 (1975).
 [20] D. Saint-James, G. Sarma, and E. J. Thomas, Type II Superconductivity (Pergamon, New York, 1969).
 [21] H. Adachi and R. Ikeda, in preparation.
 [22] H. Adachi and R. Ikeda, presented in Int. Conf. LT 23 (Physica C, in press).
 [23] Y. Kato and N. Nagaosa, Phys. Rev. B 48, 7383 (1993).
 [24] J. Hu and A. MacDonald, Phys. Rev. B 49, 15263 (1994).
 [25] R. Ikeda, T. Ohmori, and T. Tsuneto, J. Phys. Soc. Jpn. 59, 1397 (1990).
 [26] T. J. Lee, M. J. Naughton, G. M. Danner, and P. M. Chaikin, Phys. Rev. Lett. 78, 3555 (1997).
 [27] T. Shibauchi et al, Phys. Rev. Lett. 86, 5763 (2001).
 [28] R. Ikeda and H. Adachi, J. Phys. Soc. Jpn. 69, 2993 (2000).